JOURNAL OF GEOPHYSICAL RESEARCH, VOL. 100, NO. A9, PAGES 17,429–17,442, SEPTEMBER 1, 1995

Structure of auroral precipitation during a theta aurora from multisatellite observations

Y. I. Feldstein,[1] P. T. Newell,[2] I. Sandahl,[3] J. Woch,[3,4] S. V. Leontjev,[5] and V. G. Vorobjev[5]

Abstract. A θ aurora previously discussed on the basis of Viking images (northern hemisphere) and DE 1 images (southern hemisphere) is reexamined in light of additional data, primarily the auroral plasma distribution as determined from the Viking, DMSP F6, and DMSP F7 satellites. This event, which occurred before a substorm expansion phase on August 3, 1986, appeared in the images to consist of a single arc along the morning side in the northern hemisphere and along the evening side in the southern hemisphere and was isolated from the auroral oval in both sets of images. On the basis of the auroral plasma distribution inferred from three satellites, the brightest arcs do occur at the locations indicated by the imagers, but the arcs are in fact connected to the main oval with continuous precipitation, and weaker secondary arcs (not observed by the imagers) occur in the opposite hemisphere magnetically conjugate to the bright arcs. These observations support the interpretation of the θ aurora as occurring on closed field lines as a result of the expansion of the morning and evening sector ovals into the polar cap. A careful examination of the characteristics of the observed auroral energy plasma suggests additional conclusions. It appears that the ionospheric manifestation of the recently discovered low-energy electron layer can be identified with a complicated structure of soft precipitation at the poleward edge of the main precipitation region. Finally, unlike recent reports, the ions were not observed to have a cutoff in the polar cap that is any sharper than that of the electrons.

1. Introduction

The θ aurora has been interpreted as representing a bifurcation of the plasma sheet [*Frank et al.*, 1986], an interpretation that implies a region of open field lines separating the θ aurora from the main auroral oval. Conversely, *Meng* [1981], *Murphree and Cogger* [1981], and *Lundin et al.* [1991] have interpreted polar arcs as representing an expansion of the closed auroral field lines poleward, especially in the dawn and dusk sectors. *Hones et al.* [1989] further developed this interpretation observationally and theoretically and showed that a "horse-collar" auroral pattern, in which two "bars" or sun-aligned polar arcs exist along the poleward edge of the expanded morningside and eveningside auroral ovals, is a common situation for magnetically quiet times.

Observational support for these models has been mixed. *Mizera et al.* [1987], using precipitation data from NOAA 7 (southern hemisphere) and DMSP F6 (northern hemisphere) satellites, found that bursts, which they believed to be θ auroras, occurred simultaneously in both hemispheres. *Obara et al.* [1988] concluded that a polar arc imaged by Viking in the northern hemisphere was conjugate to particle measurements from Exos C measurements in the southern hemisphere. These results support an expansion of closed auroral field lines poleward to explain polar arcs and θ aurora. However, *Craven et al.* [1991] studied an instance of θ aurora before the expansion phase of a substorm on August 3, 1986, using the Viking (in the northern hemisphere) and DE 1 (in the southern hemisphere) imagers. This occurrence is the only known example of imaging both hemispheres during a θ aurora. The images indicated that a single sun-aligned polar arc existed along the morning (evening) sector in the northern (southern) hemisphere, with both arcs separated from the main auroral oval by regions without luminosity. These results of *Craven et al.* [1991] support the interpretation of *Frank et al.* [1986] of the θ aurora as representing a bifurcation of the plasma sheet with open field lines separating the θ aurora from the auroral oval.

The distribution of auroral energy plasma (hundreds of eV to several keV) in the magnetosphere is among the most important characteristics of the global magnetospheric morphology. At present, the large-scale structure and dynamics of auroral luminosity and particle precipitation in the ionosphere and the issue of mapping these regions to the outer magnetosphere are under active discussion [e.g., *Stasiewicz*, 1991; *Weiss et al.*, 1992; *Elphinstone et al.*, 1993a]. In this paper we reexamine the August 3, 1986, event using particle data from the DMSP F6 and F7 and Viking satellites to investigate these and related issues. Be-

[1]Institute of Terrestrial Magnetism, Ionosphere and Radiowave Propagation, Troitsk, Russia.
[2]Applied Physics Laboratory, Johns Hopkins University, Laurel, Maryland.
[3]Swedish Institute of Space Physics, Kiruna, Sweden.
[4]Now at Max-Planck-Institut für Aeronomie, Lindau, Germany.
[5]Polar Geophysical Institute, Apatity, Russia.

Paper number 95JA00379.
0148-0227/95/95JA-00379$05.00

cause of the recent advancements in understanding the mapping of the magnetotail into the auroral oval and to make our interpretation of the particle data clearer, a review of current understanding of particle precipitation regions and their relationship to high-altitude structures on the nightside is presented in the remainder of this section.

The structure of the high-altitude magnetotail has been established from comprehensive in situ measurements [e.g. *Eastman et al.*, 1984; *Parks et al.*, 1992]. It contains the central plasma sheet (CPS), the main body of hot, nearly isotropic plasma in the tail; the plasma sheet boundary layer (PSBL) with field-aligned, velocity-dispersed particle beams at the outer edge of the CPS; and a low-energy electron layer (LEL) at the outer edge of the PSBL with an outward electron beam and an earthward beam of ions, both at energies of a few hundred eV or less. The CPS is located on each side of the neutral sheet in the magnetotail, on magnetic field lines that are stretched in the antisunward direction. The earthward boundary of the CPS lies close to the boundary of stable trapping for high-energy particles (or the isotropic boundary). On the nightside it defines a narrow transition shell region between the quasidipolar magnetic field of the inner magnetosphere and taillike, stretched field region farther down the tail. This transition shell region is due to the inner edge, or a strong outward gradient, of the integrated cross-tail current of the plasma sheet.

The region of the inner magnetosphere extending inward from the trapping boundary to the zero-energy convection boundary, or the plasmapause, was named the remnant layer (RL) by *Feldstein and Galperin* [1985, 1993] and *Elphinstone and Hearn* [1993]. Continuous convection and plasma injection during substorms transport low-energy particles into this region. Therefore they can be considered as remnants of the plasma sheet within the region of energetic particle trapping.

The authors have discussed their view of magnetospheric topology and how these high-altitude structures map to the ionosphere at some length elsewhere [*Feldstein and Galperin*, 1985; *Galperin and Feldstein*, 1991; *Feldstein et al.*, 1994a]. Those who wish more detail on magnetospheric topology and its mapping to the ionosphere are referred to these papers. Because of the complex structure of the magnetospheric plasma sheet, we will herein refer to the precipitation structure in neutral (purely descriptive) terms that do not contain implicit mapping assumptions to be sure that our views of the mapping suggested by the evidence are included but not embedded in the nomenclature.

Broadly speaking there exist three major regions of nightside precipitation (in order of increasing latitude):

1. This first region is the diffuse auroral electron precipitation on the background of the outer radiation belt electrons up to the stable trapping boundary. Through much or sometimes all of this region the electron energy increases with latitude. This region will be termed "diffuse precipitation" (DP).

2. The second region is hard structured electron and isotropic ion precipitation between 1 and 10 keV, poleward of the stable trapping boundary. This region will be termed "hard precipitation" (HP).

3. The last region is soft structured electron precipitation with low intensity and typical energies < 1 keV. This region, which is poleward of the main auroral oval, is termed "soft precipitation" (SP).

In magnetically quiet intervals, polar arcs may exist up to very high latitudes, filling up much of the polar cap. This factor complicates determining the poleward boundary of the auroral oval and the softer precipitation region on the basis of auroral electron data only, since their spectra in these two regions above the discrete auroral forms are very similar [*Murphree et al.*, 1983; *Peterson and Shelley*, 1984; *Frank et al.*, 1986]. Arguing for the existence of systematic differences between ion precipitation in the auroral oval and poleward of it, *Troshichev and Nishida* [1992] and *Gusev and Troshichev* [1992] suggested that the ion precipitation drop-off allows a better determination of the auroral oval poleward boundary. These authors argued that the ion flux levels dropped off much more sharply poleward of the auroral oval than did the electrons.

With development of a magnetic disturbance the polar arcs poleward of the auroral oval disappear, but poleward of the highest latitude auroral oval arc a narrow band of soft particle precipitation remains. The result is a faint luminosity, which has been called polar diffuse aurora (PDA) [*Eather and Akasofu*, 1969]. Precipitation in this region as a rule is structured. Because of the relatively low intensity of PDA precipitation, the luminosity is subvisual, and the spectrum is softer than in the auroral oval. As a result the luminosity is at higher altitudes and is redder. Such luminosity was identified in pioneering papers by *Eather* [1969] and *Eather and Mende* [1972], based on airborne photometric observations with relatively poor spatial resolution. Despite the name, there is evidence that PDA includes structured fluxes. The character of the auroral luminosity and structured precipitating soft auroral electron fluxes poleward of the large-scale polar arcs were described by *Austin et al.* [1993] using Viking data. The width of this region varies from several tens to several hundreds of kilometers. Relying on particle data taken from the DMSP satellites, *Akasofu et al.* [1991] also concluded that a belt of particle precipitation exists poleward of the auroral oval. Inside this belt the auroral luminosity is so weak that it is usually not detectable in the presently available satellite auroral images. At PDA latitudes ion fluxes exist with E<10 keV and sometimes with velocity dispersed ion structures (VDIS 2) signatures characterized by ion energy decreasing toward lower latitudes [*Zelenyi et al.*, 1990].

The occurrence of bright polar arcs in the poleward region is closely connected to the geomagnetic field topology. Observations have shown that the plasma causing the luminosity of large-scale polar arcs lies on closed field lines exhibiting a double loss cone type of distribution characteristic of a trapped particle population [*Peterson and Shelley*, 1984; *Frank et al.*, 1986; *Eliasson et al.*, 1987]. Three possible morphologies of closed magnetic field lines in the poleward region have been suggested: (1) widening of the plasma sheet and luminosity region toward higher latitudes on the dawn and dusk sides [*Meng*, 1981; *Murphree and Cogger*, 1981]; (2) bifurcation of the open field lines of the polar cap by a wedge of closed field lines from which the bright emissions originate [*Frank et al.*, 1986; *Frank and Craven*, 1988]; and (3) an expansion of the low-latitude boundary layer (LLBL) [*Lundin et al.*, 1991]. In the first and third cases, one might expect an

asymmetry in the luminosity and electron fluxes across the polar arc, whereas in the second case a low level of luminosity and precipitation is observed on each side of the polar arc. The first and third cases differ on the large-scale convection direction in the vicinity of the arc; namely, in the first case, convection reverses on both sides of the arc, whereas in the third case, convection is antisunward throughout the arc and on both sides [cf. *Weiss et al.*, 1993].

Examining Viking and DMSP auroral images as well as the corresponding particle data, *Austin et al.* [1993] and *Makita et al.* [1991] both reported the existence of polar arcs on the poleward edge of the soft precipitation region. This region extends from the dawn (dusk) sector of the auroral oval precipitation for interplanetary magnetic field (IMF) $B_y < 0$ (>0) in the northern (southern) hemisphere. Movement of polar arcs is also controlled by the IMF B_y sign: along the B_y direction in the northern hemisphere and opposite to it in the southern hemisphere [*Craven and Frank*, 1991]. The asymmetry in θ aurora location relative to the noon–midnight meridional plane in both hemispheres [*Craven et al.*, 1991] or θ aurora and associated plasma in the magnetotail lobe [*Huang et al.*, 1989] suggest conjugacy with a mirror reversal between hemispheres. Such mirror conjugacy can be interpreted as the result of the IMF B_y influence on the location of reconnection regions between the interplanetary magnetic and geomagnetic field lines in the northern and southern hemispheres.

Section 2 contains a brief description of satellites and instruments and presents data about the precipitation morphology. Discussion and interpretation follow in section 3, with the conclusions given in section 4.

2. Instrumentation and Observations

Viking plasma instrumentation consists of seven spectrometer units, of which three have been used herein. These measured the directional electron flux over the energy range 0.01–200 keV and ion flux over the range 0.04–40 keV. A detailed description is given by *Sandahl et al.* [1985]. The satellite moved along the orbit with 13,530-km apogee and 817-km perigee at an inclination of 98.8°.

The DMSP satellites measure fluxes of electrons and ions within the 0.032–30 keV energy range [*Hardy et al.*, 1984]. Since detector apertures are always oriented toward the zenith, only particles well inside the loss cone are observed at the latitudes of interest herein. One full spectrum is obtained per second. Both the DMSP F6 and F7 satellites move in sun-synchronous, nearly circular orbits of 835-km altitude.

2.1 Precipitation Structure as Observed by Viking

We consider first a Viking pass through the high-latitude region on August 3, 1986, between 1710 and 1930 UT, which crossed high latitudes from the prenoon to postmidnight local time sectors. The location of auroral precipitation boundaries at high latitudes is closely related to interplanetary parameters, particularly the B_z and B_y components. Figure 1a shows the IMF variations as measured by the IMP 8 satellite, located at (32.5,−13.5,−15.4)

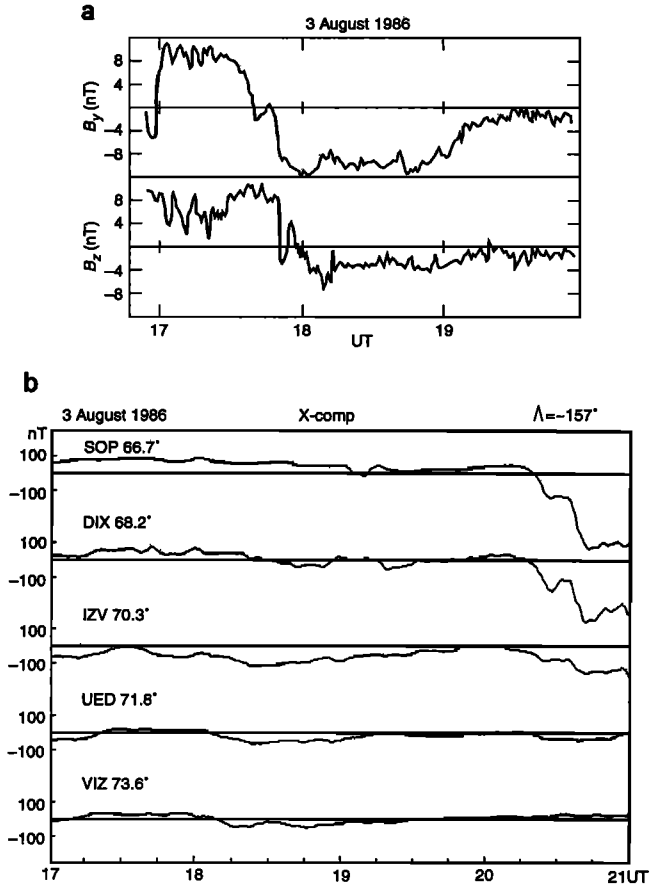

Figure 1. (a) B_y and B_z components of the interplanetary magnetic field (IMF) as measured by IMP 8 on August 3, 1986. (b) Variations of the geomagnetic field x component along a meridional chain of magnetic stations (intermediate latitude [ILAT], geomagnetic longitude): Sopochnaya (SOP; 66.7°,157.4°); Dixon Island (DIX; 68.2°,155.8°); Izvestiya Island (IZV; 70.3°,158.8°); Uedinenia Island (UED; 71.8°,158.8°); Uyze Island (VIZ; 73.6°,156.2°).

(x,y,z in R_E). The B_y (B_z) components vary from +10 nT (+8 nT) at the start of the aforementioned interval to −10 nT (−2 nT) by the end of the interval. A transition of the IMF B_y (B_z) components from one sign to the opposite took place at 1750 (1800) UT.

Figure 1b presents the variation of the geomagnetic field x component for a chain of magnetic stations near 2400 magnetic local time (MLT) along 157° geomagnetic meridian. A substorm expansion phase began at 2015 UT with a sharp decrease of the x component at auroral zone stations (67–68°). Indications of a growth phase had previously been observable since about 1800 UT throughout the latitudinal chain. Specifically, clear x component decreases were noted for stations located poleward of the auroral zone (70–72°), which coincides with the IMF southward turning. During the Viking pass an increase in the AU and *AL* indices was recorded. Thus the Viking pass includes a magnetically quiet interval prior to 1800 UT and also the early stages of a growth phase up to 1930 UT (45 minutes before expansion onset).

Until 1828 UT, Viking measured fluxes consistent with the plasma mantle [*Newell et al.*, 1991] corresponding to a

furthest poleward position of 84.8° invariant latitude (ILAT)/917 MLT. Thereafter, fluxes dropped below the one count per readout threshold (6×10^{-3} ergs cm^{-2} s^{-1} sr^{-1} keV^{-1} for electrons and 5×10^{-5} erg cm^2 s^{-1} sr^{-1} keV^{-1} for ions). This region, which was devoid of precipitation, is considered to be the polar cap. Figure 2 shows a Viking energy-time spectrogram for electrons (top) and ions (middle) starting from 1830 UT, when the satellite was still inside the polar cap. Allowing ~20 min lag time for the IMF observed by IMP 8 to the Viking observation point (consisting of propagation times of 7 min to the bow shock, 4 min to the magnetopause, and 9 min delay in the response of geophysical phenomena [*Clauer and Banks,* 1986; *Greenwald et al.,* 1990]), it is believed that for the data presented in Figure 2, the pertinent IMF conditions are $B_z < 0$ and $B_y < 0$. During the first part of the orbit, prior to ~1841 UT, the ion detector experienced so much noise in the channels between 1.2 and 40 keV that this portion of the data was not useful.

At 1836 UT the satellite first recorded auroral plasma fluxes, namely electrons with energy 0.2–0.3 keV and fluxes up to 10^5 e- cm^{-2} s^{-1} sr^{-1} eV^{-1} and ions with energy 0.5 keV and flux of about 5×10^2 ions cm^{-2} s^{-1} sr^{-1} eV^{-1}. Auroral plasma with such parameters was observed until 1837 UT (85.0° ILAT/0728 MLT) when both the energy and flux of electrons increased to 0.5 keV and 10^6 e- cm^{-2} s^{-1} sr^{-1} eV^{-1}, respectively. Apparently, it was the first encounter of Viking with the plasma above the θ aurora. A θ aurora was distinctly discerned in Viking images up to 1828 UT when optical observations in the northern hemisphere ceased, whereas in the southern hemisphere the DE 1 satellite recorded auroras up to ~20 UT [*Craven et al.,* 1991].

The belief that this encounter was with the θ aurora is confirmed by calculating the motion of the θ aurora following the imager observation. The direction of the motion of the luminosity band is determined from the sign of B_y [*Craven and Frank,* 1991], whereas the velocity of the θ aurora in the southern hemisphere was observed by all-sky camera [*Feldstein et al.,* 1992]. The resulting computation indicates that the Viking trajectory transversed the θ auroral band at ~1837 UT. Figure 3 shows the observed θ aurora locations in the northern hemisphere at three times: (1) 1756 UT, (2) 1819 UT, and (3) 1826 UT [*Elphinstone et al.,* 1993b]. The velocity of the θ aurora shift during this time is ~0.4 km s^{-1} according to all-sky camera observations at Vostok station. The expected location of the θ aurora at 1837 UT is shown by "4," and the position of the Viking satellite at 1837 UT is given by a cross.

Both the luminosity band and Viking move toward the dawn side from the noon–midnight meridian. This shift and the complicated structure of the luminosity band incorporating three auroral arcs naturally explain multiple increases in the auroral fluxes up to 1906 UT (75.9° ILAT/0325 MLT) seen in the spectrogram. Figure 3 also shows ("5") the location of the θ aurora expected based upon reflecting the southern hemisphere observations about the noon–midnight meridian [*Craven et al.,* 1991]. Between 1837 UT and 1906 UT, Viking observed ions with energies from 1 to 10 keV and with a flux below 10^3 ions cm^{-2} s^{-1} sr^{-1} eV^{-1}. An increase in the electron flux is accompanied by low-energy, high-intensity upward ion beams. With the exception of an upward loss cone above 1 keV, the ion population is isotropic, whereas the electron population has a highly varying flux level and pitch angle characteristics. After 1906 UT, only faint and sporadic electron beams appear, and from 1911 UT (73.6° ILAT/0318 MLT) up to 1918 UT (69.4° ILAT/0302 MLT) the electron flux was near instrument threshold. The ion fluxes subside as well, with their spectra becoming softer, and the ion beams disappear. For a detector with a comparatively high threshold, this region might be considered empty polar cap. However, detailed analysis of the ion spectra shows that a flux of $\sim 3 \times 10^2$ ions cm^{-2} s^{-1} sr^{-1} eV^{-1} of isotropic ions with energies above 1 keV still exists. This flux is slightly above the spectrometer threshold and indicates continuity of auroral plasma precipitation along the Viking pass, though characteristics of fluxes may vary substantially.

After 1918 UT the intensity of auroral plasma fluxes begins to increase. In the interval until 1921 UT (67.5° ILAT/0256 MLT) at the height of ~8400 km, structured bursts of soft electrons with E< 1 keV occur, but ion fluxes remain at low levels. Around 1921 UT a sharp increase of structured fluxes and energy of precipitating electrons takes place. At the poleward edge of this region, ion fluxes also increase, beginning with higher energies. Such characteristics of this event as its location at the poleward boundary of intense, structured electron precipitation, and the latitudinal character of the ion energy dispersion justify identification as VDIS 2.

In the UT range 1921–1927 UT (63.2° ILAT/0242 MLT), Viking, at 7500-km altitude, intersected the region of harder electron precipitation with electron energy E_e up to several keV, namely the discrete auroral oval. The high-energy electron channels indicate that the stable trapping boundary Φ_s, which terminates the outer radiation belt and which *Feldstein and Galperin* [1985] have argued divides the diffuse aurora from discrete, is encountered at 1927 UT. Fluxes of ions with $E_i \approx 10$ keV sharply increase and are isotropic except for the upward ion loss cone. At 1927 UT the ion distribution changes from basically isotropic to a double loss cone. After 1927 UT a characteristic decrease of maximum energy electrons is observed.

Magnetic field measurements show that the character of the field-aligned currents also changes at the boundary between HP and DP, as previously noted at other local times [*Potemra,* 1977; *Erlandson et al.,* 1991]. Poleward (equatorward) of this boundary, the currents are directed inward (outward) of the ionosphere, which corresponds to the Region 1 (Region 2) currents of *Iijima and Potemra* [1976]. In the equatorward portion of the large-scale inward current, small-scale but intense local outward field-aligned currents were observed, corresponding to individual discrete auroral forms.

The boundary of bursty precipitating electrons with up to tens of keV energy and decreasing intensity with increasing latitude occurred at ~1921 UT. This is the background boundary (Φ_b) of energetic electron precipitation and coincides with the auroral oval poleward boundary. The location of the auroral oval poleward boundary is simply and unambiguously determined based on both electrons and ions. Though the intensity of ions in the polar cap is lower than in the auroral oval, it should be stressed that significant ion fluxes exist inside the polar cap in the vi-

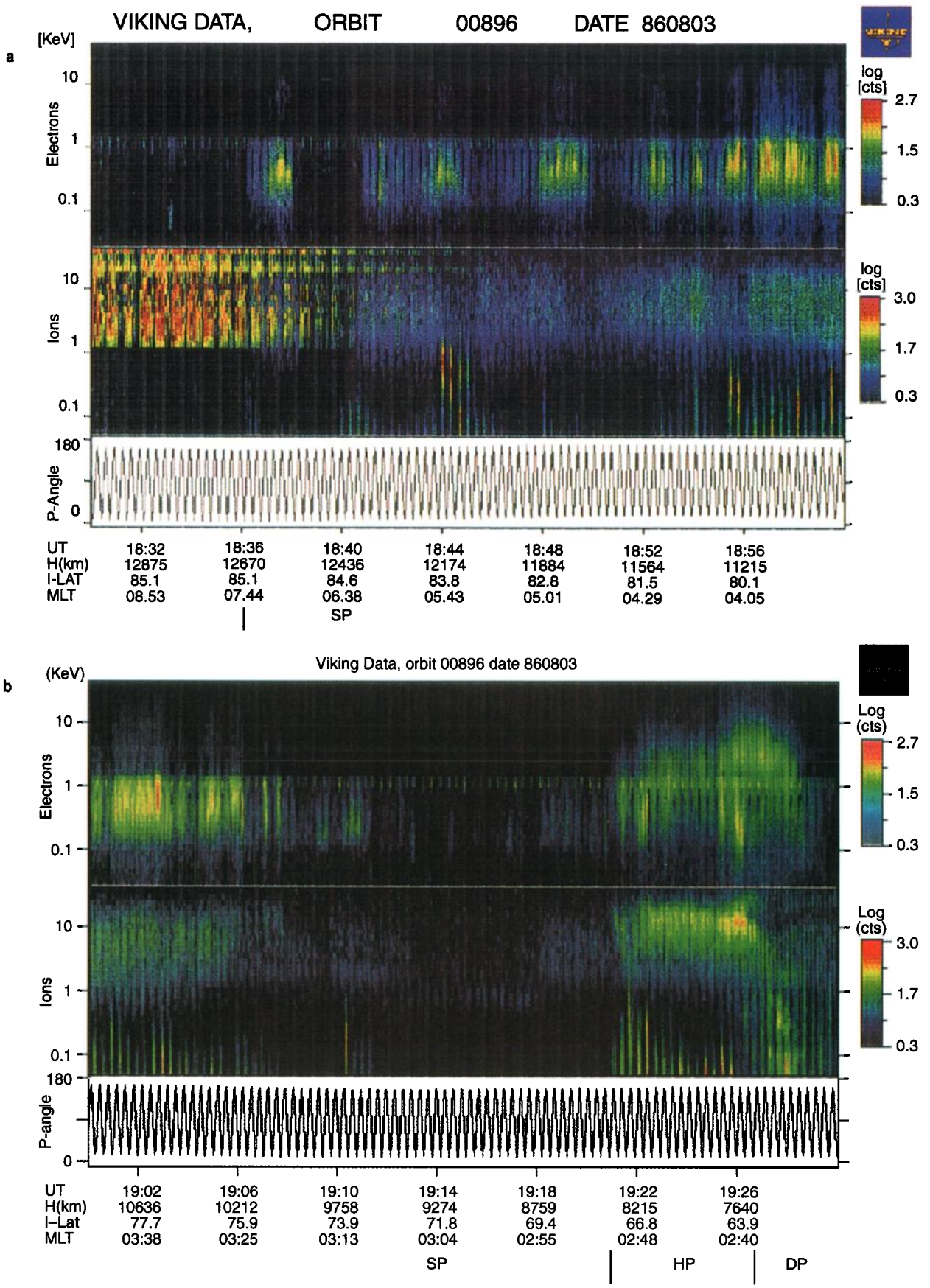

Figure 2. A spectrogram of Viking data from pass 896 in the interval from 1830 UT to 1930 UT, August 3, 1986. Electrons are at top, ions are in the middle, and pitch angles are at the bottom; the plotted count rate is proportional to the differential energy flux in arbitrary units.

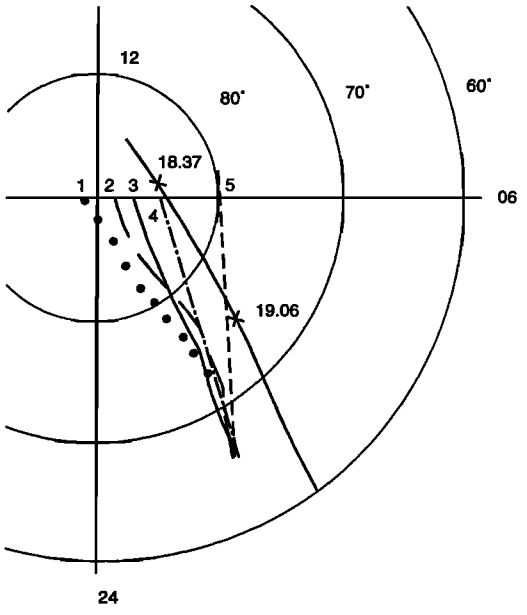

Figure 3. Successive locations of the central portion of the θ aurora in Viking images for (1) 1756 UT, (2) 1819 UT, and (3) 1826 UT. The position at (4) 1837 UT is estimated from all-sky camera observations. The position at (5) 1906 UT is that of the mirror reflection about the noon–midnight meridian of the θ aurora observed by DE 1 in the southern hemisphere. The two crosses mark the Viking satellite location at 1837 and 1906 UT.

cinity of the θ aurora. The variability of plasma fluxes observed in the vast region poleward of the auroral oval testifies to the complicated structure of the plasma region at the periphery of the plasma sheet in the magnetospheric tail.

2.2 Precipitation Structure as Observed from DMSP F6 and F7

Figures 4 and 5 present the spectrograms of precipitating electrons and ions by DMSP F6 and F7, respectively, and Figure 6 shows the satellite trajectories in polar projection and auroral oval and the location of UV auroras based on Viking and DE 1 images from 1814 to 1824 UT. Figure 4 shows that F6 crossed through the high-latitude night sector region from dawn to dusk. In the interval 1826:30 (61.5° MLAT/0425 MLT)–1827:49 UT (65° MLAT/0417 MLT), weak fluxes of soft electrons with increasing energy with increasing latitude occur (DP). This is the region of stable trapping (the outer radiation belt), since any precipitation of auroral energy ions is absent. In the interval 1827:49–1828:49 UT (67.5° MLAT/0338 MLT) the flux of precipitating electrons with several keV energy substantially increases, with such flux constituting luminosity along the auroral oval (HP). Some of the electron spectra in this interval show signs of acceleration.

In the interval 1828:49–1838:05 (67.7° MLAT/2112 MLT), structured precipitation of soft electrons with $E_e < 1$ keV was observed, superimposed on bursty electrons of higher energy associated with polar arcs as well as ion precipitation with $E_i \sim 1$–10 keV (SP). Between the dawn sector auroral oval and the electron bursts above the polar arcs, there exists continuous precipitation. Most intense bursts take place over an interval 1830:45–1831:40 UT, with the maximum energy flux at 1831:22 UT (72.7° MLAT/0150 MLT) and at 1834:10–1834:42 UT, with a peak energy flux value at 1834:13 (74.1° MLAT/2330 MLT). These bursty locations are marked by thick lines along the satellite trajectory. Within this interval some electron spectra show signs of "monoenergetic peaks," indicating acceleration by field-aligned potential drops. The energy flux and average energies are lower during the second burst than in the first.

The region of structured soft precipitation is not continuous along the satellite trajectory from the dawn sector to the dusk sector. Over the interval 1834:57 UT (74.0° MLAT/2305 MLT)–1836:15 UT (71.4° MLAT/2210 MLT), very soft electron and ion precipitation without bursts of electrons was observed. The character of fluxes and their energy spectra in this region were similar to that described above from Viking data in the interval 1911–1918 UT. It seems likely that the satellites intersected the soft precipitation region from the plasma sheet periphery.

At 1838:05 UT the energy of the electrons sharply increased, and a region of hard precipitation with high ion fluxes in the range ~10 keV is observed, which reaches to 1838:35 UT (66.5° MLAT/2100 MLT), the HP. The subsequent decrease of auroral electron flux and energy before 1839:02 UT (64.8° MLAT/2052 MLT) is a consequence of the satellite's entry into the diffuse precipitation region.

In the morning and night sectors DMSP F7 crossed high latitudes. Over the interval 1836:27 UT (69.4° MLAT/0648 MLT)–1839:41 UT (74.5° MLAT/0449 MLT), auroral energy electron and ion precipitation are intense and structured (MP in Figure 5). The location of the precipitation region in the dawn sector suggests a connection with the boundary region of the magnetosphere in the deep magnetotail flanks [*Feldstein et al.*, 1994a].

Precipitation from 1839:41 UT to 1840:12 UT (74.6° MLAT/0421 MLT) substantially differs from precipitation that occurred directly poleward; namely, auroral electrons are virtually absent, whereas low-energy ions (0.1–1 keV) are present. Their spectral characteristics are akin to the Viking data from 1911 to 1918 UT and the F6 observations from 1834:57 to 1836:15 UT, which were classified as soft but unstructured precipitation. The location of this high-latitude region suggests a probable origin in the periphery of the magnetospheric plasma sheet region, though plasma spectral characteristics are not unlike those originating in the plasma mantle.

Beginning with 1840:12 UT, fluxes of more energetic electrons and ions appear, initially relatively homogeneous in character but distinctly structured from 1840:50 UT (74.6° MLAT/0355 MLT) until 1847:34 UT (64.5° MLAT/00:00 MLT). This latter interval is the region of soft structured precipitation (SP). Three particularly strong bursts of electron precipitation with accompanying intensification of ion fluxes in the energy range $E_i \sim 1$–10 keV take place between 1841:19 and 1842:34 UT. This interval is marked by the thick line in Figure 6 on the DMSP F7 trajectory and corresponds to a θ aurora from the Viking image. Particle precipitation clearly demonstrates that the "bar" in the θ aurora has a fine structure and actually consists of several polar arcs. The fine structure of the θ aurora for August 3, 1986, was first shown by *Feldstein et al.* [1992]

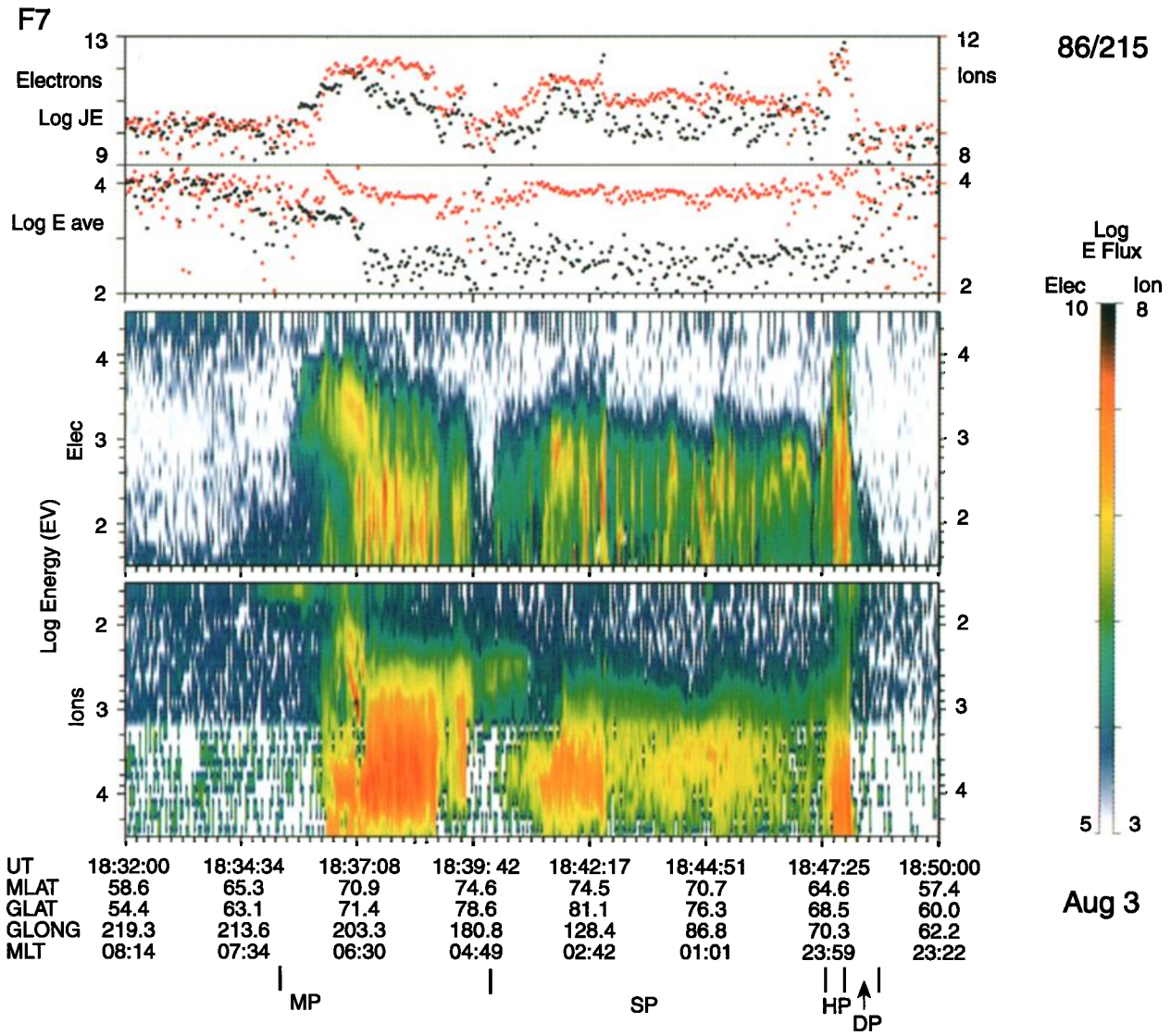

Figure 4. Spectrogram of DMSP F6 particle observations in the interval 1825 UT to 1843 UT. The spectrogram shows differential energy flux from 32 eV to 30 keV in units of eV/(cm² s sr eV). The top line plot shows total energy flux (eV/cm² s sr), and the bottom line plot shows average energy (eV). Note that the ion energy scale is inverted.

based on all-sky camera observations in the southern hemisphere. At 1847:34 UT the satellite intersected an intense auroral arc, judging from the sharp increase of both electron and ion fluxes over a wide energy spectral range of up to tens of keV (HP). The auroral arc equatorial boundary was intersected at 1848:04 UT (62.7° MLAT/2350 MLT), and the arc location is in good agreement with the Viking image. The hard precipitation region comprises a very narrow latitudinal interval, as is typical for intervals that follow an IMF southward turning but are prior to a magnetospheric substorm expansion onset. Equatorward of the hard precipitation, the spectrum of auroral electrons becomes abruptly softer, with maximum energy decreasing with latitude and ion precipitation absent. This is the outer radiation belt region, which is characterized by diffuse precipitation (DP).

The bursts of electron precipitation with $E_e > 1$ keV are responsible for generating polar arcs at high latitudes inside the auroral oval. The SP region has apparently a complicated structure with soft structureless precipitation at very high latitudes. It is possible that such a precipitation is connected with the plasma sheet periphery in the magnetospheric tail. Passes by DMSP F6 and F7 show the existence of intense ion fluxes in the polar cap. Counter to the suggestions of *Troshichev and Nishida* [1992] no sharp dropout of ions in the polar cap is observed. Thus the determination of the poleward auroral oval boundary based on ion observations affords no advantage over the more standard usage of electron data.

3. Discussion

Observations of the auroral plasma during an interval in which the IMF turned southward but well before any substorm onset show that precipitation in the dawn and night sectors occurs practically continuously inside the

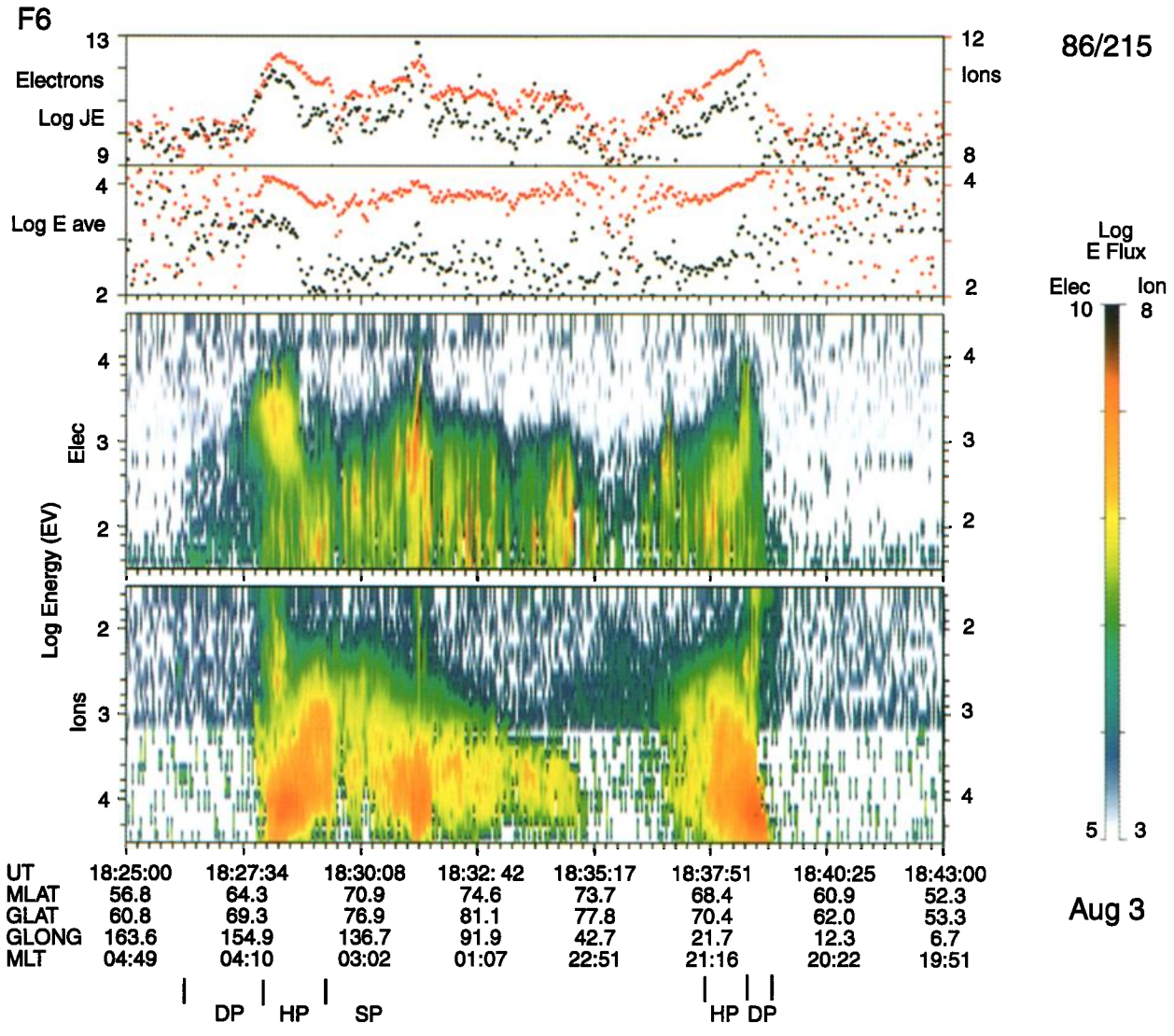

Figure 5. A DMSP F7 spectrogram for the interval 1832–1850 UT on August 3, 1986.

wide interval of latitudes from the auroral oval to 85°. Thus for this particular case the full set of detailed observations better corresponds to the hypothesis of plasma sheet widening [*Meng,* 1981; *Murphree and Cogger,* 1981] than bifurcation [*Frank et al.,* 1986]. However precipitation intensity may vary by orders of magnitude within the range of continuous precipitation. Figure 7 presents the variations in the electron energy flux along the Viking pass in the energy range 40 eV–30 keV, along with their mean energy, currents, and plasma density. The energy flux has a sharp maximum of 9 mW m^{-2} at the boundary between DP and HP at 1927 UT and drops off from this value moving either equatorward or poleward. Fluxes have a local maxima of several milliwatts per square meter above the polar arcs in the interval from 1837 to 1906 UT. The region with polar arcs is distinctly discerned from the auroral oval region by its intensity of both electron and ion precipitation. An interesting fact about the large-scale field-aligned current distribution should be stressed, namely that inside the auroral oval, current flows out of the ionosphere, whereas in the general vicinity of the polar cap arcs, the large-scale current flows into the ionosphere (of course, precisely above the arcs, small-scale currents are upflowing). Such interrelated location of the field-aligned currents corresponds to the widely known pattern found by *Iijima and Potemra* [1976], namely that in the dawn sector the inflow currents lie poleward of the outflow currents. The region of inflowing currents is here widened and shifted far to the poleward region. The large-scale inward current region also contains small-scale but intense outflowing currents that apparently are connected with precipitation above the polar arcs.

If the particle detectors had had a relatively high threshold (or were plotted on an insensitive scale), the decrease of particles in the interval from 1911 UT to 1918 UT could be mistaken for a discontinuity in precipitation between the auroral oval and the θ aurora, although no such discontinuity exists, either in the electron or ion data. Figure 2 presents the weak low-energy ion precipitation in this region. In Figure 8, ion spectra for the time interval 1912:00–1912:40 UT (one satellite spin period) are shown. The spectra have been binned and averaged for the pitch

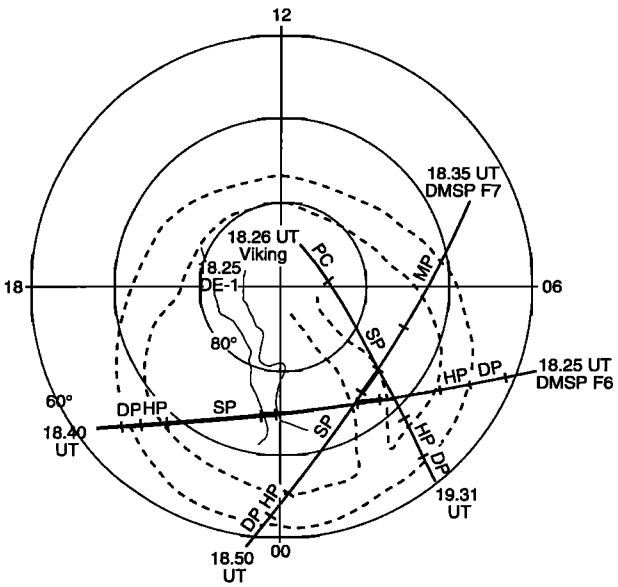

Figure 6. Trajectories for the DMSP F6 and F7 and Viking spacecraft on August 3, 1986, in corrected geomagnetic coordinates. The start and end UT times are listed along with the major plasma structures: DP, diffuse precipitation; HP, hard precipitation; SP, soft precipitation; MP, morning precipitation; PC, polar cap precipitation. The bursts of auroral precipitation along the DMSP F6 and F7 trajectories are marked by heavy lines. The dashed lines mark the medium position of auroral luminosity region based on Viking images between 1814 and 1824 UT (data courtesy of R. Elphinstone). The solid line is the projection of the southern hemisphere polar arc based on a DE 1 image at 1825 UT into the northern hemisphere.

angle intervals 10–15°, 15–30°, 75–105°, and 150–170°. Spectra for 10–15° and 150–170° intervals correspond to the smallest and largest pitch angles available for this orbit. Ion fluxes are isotropic over pitch angles and slightly above detector threshold. Such isotropic distribution is characteristic for ion fluxes above the ionosphere at latitudes mapping onto field lines on the plasma sheet, which are highly stretched [*Sergeev et al.*, 1983; *Lyons et al.*, 1988].

Let us consider energy spectra for different structured plasma regions at Viking heights. The soft precipitation region poleward of the θ auroras deserves special interest, since it is presumably connected with the low-energy electron layer discovered by *Parks et al.* [1992]. Figure 9 presents electron and ion spectra in this region at 1836 UT.

For all pitch angles, electron fluxes sharply decrease for E > 1 keV, with maximum flux values observed at 200 eV to 500 eV. The pitch angle distribution shown in Figure 9a is isotropic for downgoing electrons, but upgoing electrons have only approximately 1/4 the flux, meaning a net flux into the ionosphere exists. Their intensity is enough for luminosity excitation in the several tens of Rayleigh of the atomic oxygen red line. The existence of weak diffuse auroral luminosity poleward of a polar arc [*Austin et al.*, 1993] is consistent with the observed downward flowing soft electron fluxes. At 1836 UT ion spectra are available for E < 1 keV only because of interference from other instruments. Fluxes of ions are approximately 2 orders of magnitude less than electron fluxes. For both ions and electrons, strong anisotropy is observed. The ion fluxes along the magnetic field lines flow into the ionosphere, with little return flow out of the ionosphere. The inward ion flow conforms with *Parks et al.*'s [1992] measurements of earthward flowing ions in the LEL at a distance of ~15 R_E. However, in contrast to the Viking electron observations, *Parks et al.*'s [1992] measurements show electron fluxes in the LEL directed toward the tail. This finding means that either the source of auroral electrons in the LEL is located at heights between 2 R_E and 15 R_E, or if the source lies in the magnetotail, a search for such fluxes at the periphery of the plasma sheet is appropriate. The availability of precipitating soft electrons at ~12,500-km height removes difficulty when attempting to connect *Parks et al.*'s [1992] LEL with luminosity poleward of the polar arcs region.

Let us consider the electron and ion spectra above the polar arcs. Figure 10 presents a typical spectra observed

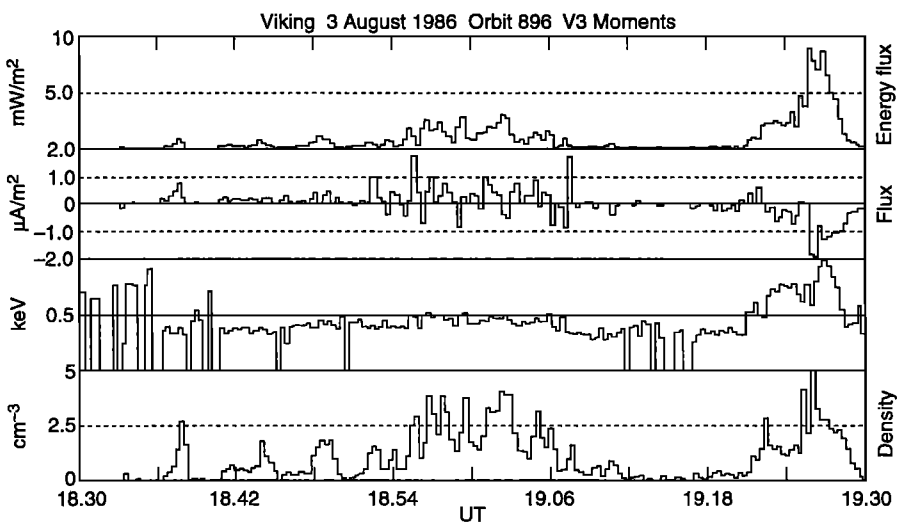

Figure 7. Summary plot of Viking data from orbit 896, August 3, 1986. The plot shows the electron energy flux, field-aligned currents (downward positive and upward negative), average electron energy, and electron density for the electron energy range 40 eV to 30 keV.

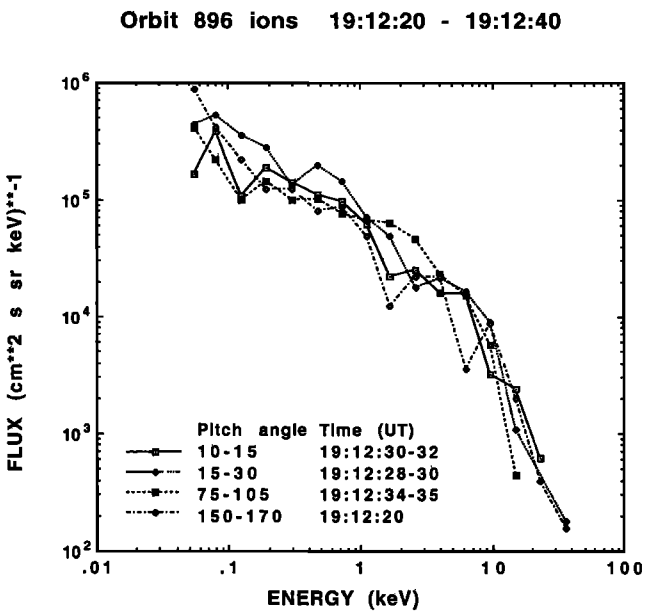

Figure 8. Ion energy spectra for the region between the auroral oval and polar arcs for different pitch angles during a 20-s interval of the satellite revolution from 1912:20 to 1912:40 UT.

from Viking (1900:23 UT). The fluxes of precipitating electrons peak at small pitch angles, with intensity reaching 10^6 e- cm^{-2} s^{-1} sr^{-1} eV^{-1} at 200 eV. The fluxes remain substantial at higher energies as well, about 10^5 at 1 keV, and gradually decrease to 10^3 at 6 keV. Above 1 keV upgoing electrons are virtually absent. The spectra ions inside and outside the loss cone are practically identical, with the fluxes subsiding from ~10^3 ions cm^{-2} s^{-1} sr^{-1} eV^{-1} at 40 eV to ~2×10^1 at 10 keV. A typical upgoing ion beam is characterized by a sharp increase of flux up to 10^4 ions cm^{-2} s^{-1} sr^{-1} eV^{-1} at 40 eV, with a sharp cutoff and virtual absence of ions with energy above 1 keV. The spectra indicate that at the satellite height of 11,000 km a field-aligned electric field exists that accelerates electrons toward the Earth and ions in the opposite direction. It also leads to the appearance of a maximum in the electron spectrum at the energy of several hundred eV.

For the auroral oval latitudes, electron spectra, presented in Figure 11 (1922:14 UT, 8200 km), differ only slightly from the spectra above the polar arcs; namely, electrons are field-aligned, with a peak in the 200–400 eV range. At the latitudes of diffuse precipitation region near the equatorial oval boundary, as shown in Figure 12 (1928:08–1928:18 UT), the electron spectrum is isotropic in the upper hemisphere, the maximum at several hundred eV disappears, and the spectrum becomes smoother. Ions with pitch angles around 90° prevail.

Observations of DMSP F6 and DMSP F7 satellites allow a comparison of the spectra of electrons above polar arcs at different heights. Figure 13 shows an electron spectrum during a burst, as indicated by the thick lines on Figure 6. The sharp maximum at several keV is a monoenergetic peak, generally interpreted to imply a potential difference of several keV above the ionosphere. A comparison with the Viking spectrograms demonstrates that most of the potential drop must lie below 2 R_E.

Figures 13a and 13b present two spectra of DMSP F6 at 1831:22 and 1834:13 UT. The first one corresponds to the position of the polar arc, as recorded in the image of Viking, with an energy flux of 10^{10} eV cm^{-2} s^{-1} sr^{-1} eV^{-1} with a peak of 3.2 keV. This polar cap arc was also observed by DMSP F7, as shown in Figures 13c and 13d (at 1841:32 and 1842:34 UT, respectively). The F7 spectra show signs of field-aligned acceleration to 1 keV and 1.4 keV, respectively. The second arc (Figure 13b) also reveals signs of field-aligned electron acceleration but only to 250 eV, with an intensity of only 3.1×10^9 eV cm^2 s^{-1} sr^{-1} eV^{-1}. This second enhancement of the energy flux in-

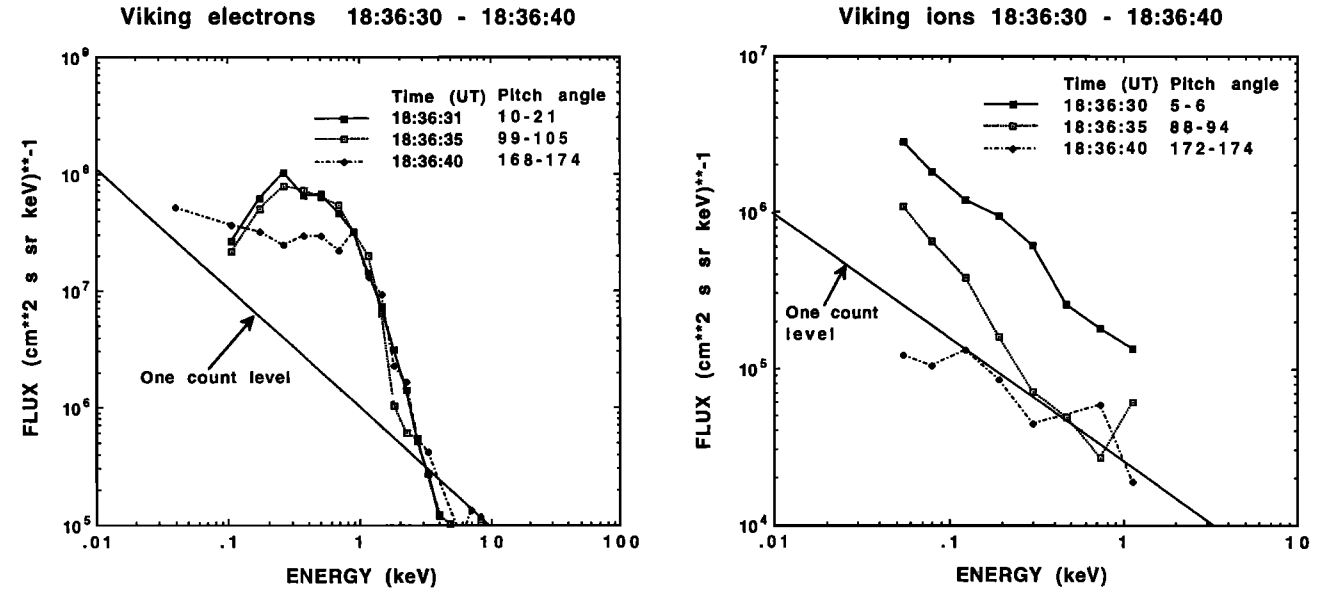

Figure 9. Electron and ion spectra observed by Viking in the region of weak diffuse precipitation poleward of a polar arc at 1836 UT. The actual time of each spectrum is the one given under UT inside the frame. The presented spectra were measured as close to the 0°, 90°, and 180° as possible.

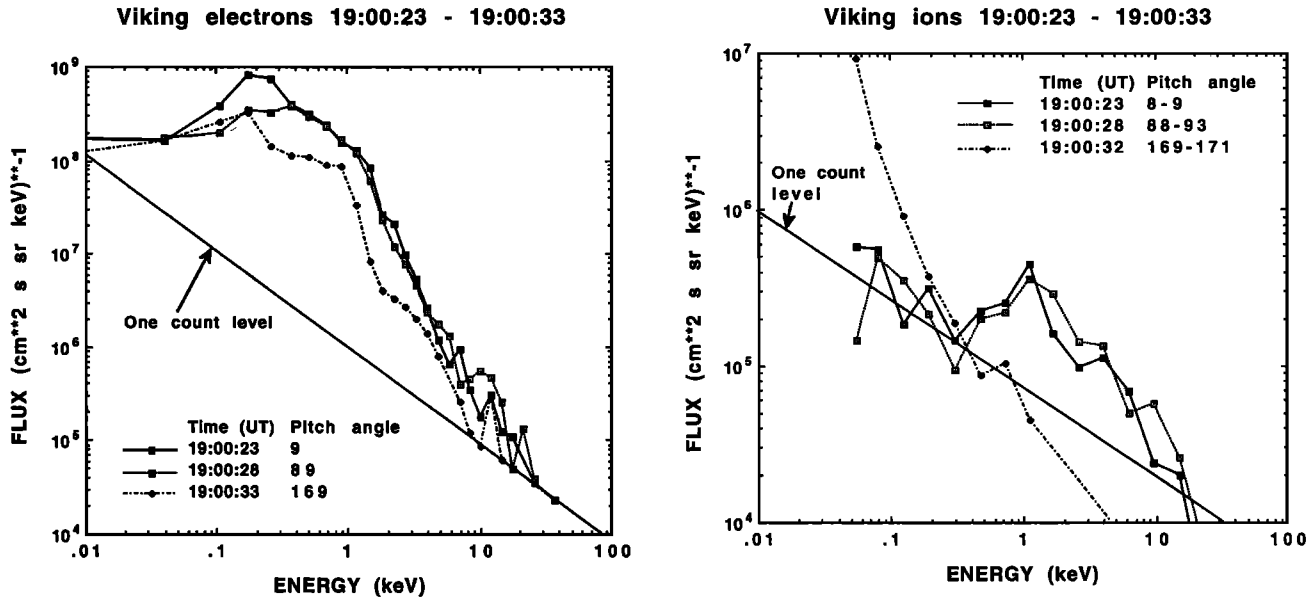

Figure 10. Electron and ion spectra observed by Viking above polar arcs at 1900 UT.

put into the ionosphere was not revealed in the Viking images until 1828 UT. However, the location of the second burst in invariant latitude-local geomagnetic time coordinates in Figure 6 precisely corresponds to the θ aurora position recorded at 1824 UT by the DE 1 satellite in the southern hemisphere [*Craven et al.*, 1991]. The correspondence is "precise" in the sense that no shift relative to the dawn–dusk plane is observed.

The absence of noticeable luminosity in the Viking image in the position of the second electron burst is due to both the lower fluxes and the softer spectrum of precipitating electrons above this second arc. According to *Elphinstone et al.* [1993b] the Viking UV camera is less responsive to fluxes of precipitating electrons whose energies are below about 500 eV. In any event, the 250-eV average energy electrons above the second polar arc are absent from the Viking images. This finding suggests that, for reliable determination of the polar cap boundary, Viking images should be supplemented by particle data.

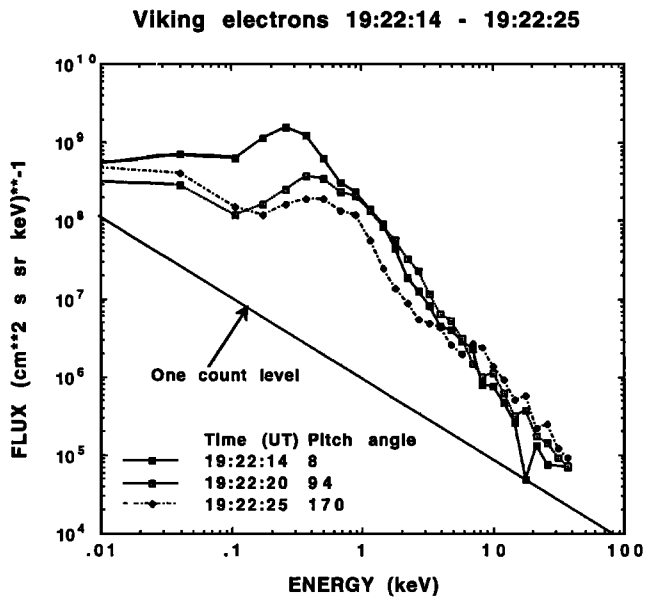

Figure 11. Electron spectra observed by Viking at auroral oval latitudes at 1922 UT.

4. Conclusions

The data presented above suggest the following interpretation. Polar arcs observed by Viking and DE 1 images presented by *Craven et al.* [1991] reflect only the positions of the most intense and energetic electron precipitation. Using particle detectors with sensitivity to lower flux inflows and apparently lower characteristic energies, a more complex luminosity structure is revealed. The conclusion of *Craven et al.* [1991] about the asymmetrical location of the θ aurora in both hemispheres on August 3, 1986, (in the morning sector in the northern hemisphere and evening sector in the southern hemisphere) is applicable only to the most intense luminosity sites (which also represent harder electron precipitation). Precipitation observations support the location of the most intense polar aurora in the northern hemisphere as being in the morning sector but show that a less intense arc occurs in the evening sector, in a conjugate position to the θ aurora observed in the southern hemisphere. Thus the precipitation pattern, but not intensity, is conjugate. The asymmetry in polar arc intensities is apparently controlled by the IMF B_y component. It is known that during intervals with $B_y < 0$ the polar cap boundary in the dawn (dusk) sector shifts poleward (equatorward) [*Elphinstone et al.*, 1990]. It is possible that the apparent shift is at least partially the consequence of a relative luminosity decrease but not actual disappearance.

The conjugacy of the polar arcs location (although not intensity) in geomagnetic coordinates and the continuity of precipitation between the auroral oval and the polar arcs both suggest that field lines above the θ aurora are closed

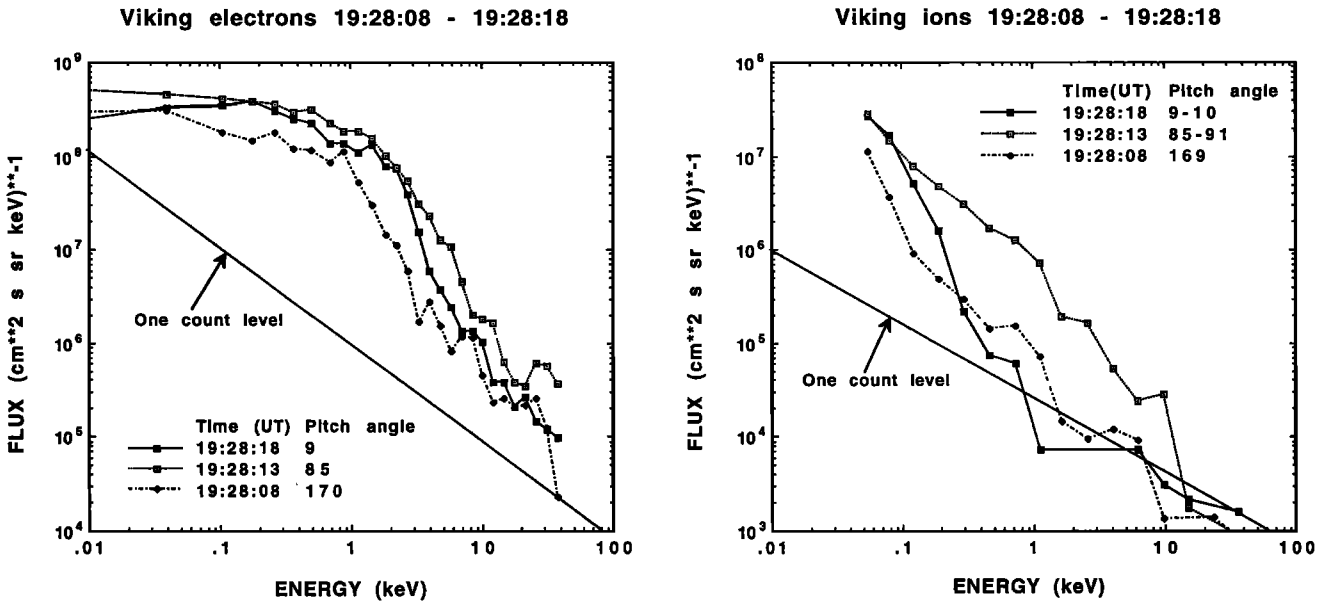

Figure 12. Electron and ion spectra observed by Viking in the diffuse precipitation region equatorward of the auroral oval at 1928 UT.

and support the hypothesis of plasma sheet widening or LLBL expansion rather than plasma sheet bifurcation to explain θ aurora. However, because electric field observations for this event [*Feldstein et al.*, 1994b] and previously reported θ aurora [*Frank et al.*, 1986] show that convection reversals occur on both sides of the θ aurora, we believe that only the hypothesis of an expanding plasma sheet adequately explains all observations. The cause of the B_y-dependent asymmetry in the intensity of the auroral precipitation is still unresolved.

Some other conclusions can also be reached from our study. Detailed examination of the precipitation characteristics immediately poleward of the main auroral oval indicates a correspondence between this region (SP or PDA) and the LEL found at high altitudes by *Parks et al.* [1992]. Finally, our observations indicate that, contrary to previous suggestions [*Troshichev and Nishida*, 1992], ions are present poleward of the auroral oval during a θ aurora event, and do not serve any better to demarcate the auroral oval boundaries than do electrons.

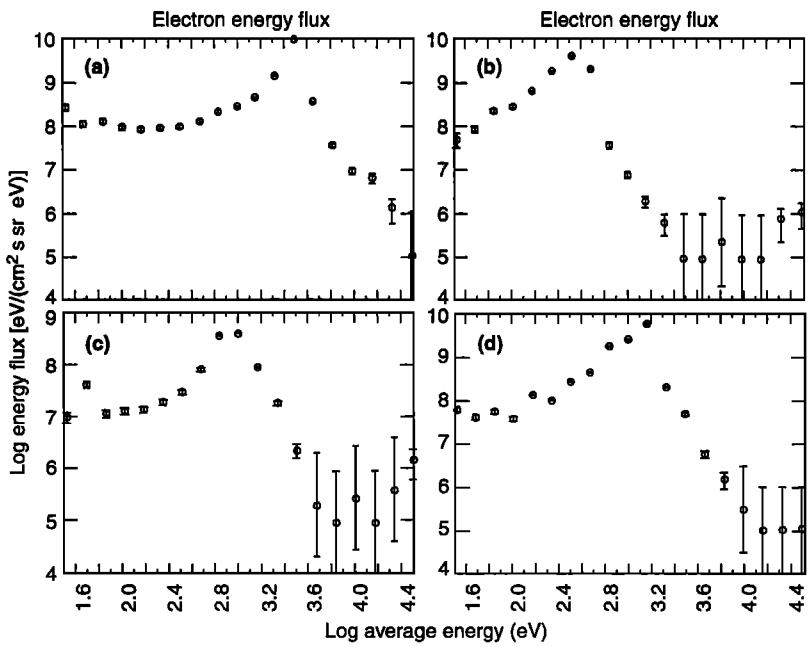

Figure 13. Electron spectra above the polar arcs on August 3, 1986, observed by the satellites DMSP F6 at (a) 1831:22 UT and (b) 1834:13 UT and DMSP F7 at (c) 1841:32 UT and (d) 1842:34 UT.

Acknowledgments. The authors thank the referees for their unusually thorough and helpful suggestions. Discussions with B. Hultqvist, J. Craven, and Y. Galperin have been useful. R. Elphinstone kindly supplied the Viking images, and O. Troshichev supplied the magnetic meridian observations. This research has been supported by the Russian Foundation for Fundamental Research at IZMIRAN by grant 93-05-8722 and at PGI by grant 94-05-16273a and by the International Science Foundation grant M6P000. Viking was financed by the Swedish Board for Space Activities and managed by the Swedish Space Corporation. Work at JHU/APL was supported by NSF GEM grant ATM-9300866.

The Editor thanks two referees for their assistance in evaluating this paper.

References

Akasofu, S.-I., C.-I. Meng, and K. Makita, Changes of the size of the polar cap during substorms (abstract), *EOS Trans. AGU, 72*(44), Fall Meeting Suppl., 400, 1991.

Austin, J. B., J. S. Murphree, and J. Woch, Polar arcs: New results from Viking UV images, *J. Geophys. Res., 98,* 13,545–13,555, 1993.

Clauer, C. R., and P. M. Banks, Relationship of the interplanetary electric field to the high-latitude ionospheric electric fields and currents, *J. Geophys. Res., 91,* 6959–6971, 1986.

Craven, J. D., and L. A. Frank, Diagnosis of auroral dynamics using global auroral imaging with emphasis on large-scale evolutions, in *Auroral Physics,* edited by C.-I. Meng, M. Rycroft, and L. A. Frank, pp. 273–288, Cambridge University Press, New York, 1991.

Craven, J. D., J. S. Murphree, L. A. Frank, and L. L. Cogger, Simultaneous optical observations of transpolar arcs in the two polar caps with DE 1 and Viking, *Geophys. Res. Lett., 18,* 2297–2300, 1991.

Eastman, T. E., L. A. Frank, W. K. Peterson, and W. Lennartson, The plasma sheet boundary layer, *J. Geophys. Res., 89,* 1553–1572, 1984.

Eather, R. H., Latitudinal distributions of auroral and airglow emissions: The "soft" auroral zone, *J. Geophys. Res., 74,* 153–158, 1969.

Eather, R. H., and S.-I. Akasofu, Characteristics of polar cap auroras, *J. Geophys. Res., 74,* 4794–4798, 1969.

Eather, R. H., and S. B. Mende, High latitude particle precipitation and source regions in the magnetosphere, in *Magnetosphere–Ionosphere Interactions,* edited by K. Folkestad, pp. 139–154, Universitatforlaget, Oslo, 1972.

Eliasson, L., R. Lundin, and J. S. Murphree, Polar cap arcs observed by the Viking satellite, *Geophys. Res. Lett., 14,* 451–454, 1987.

Elphinstone, R. D., and D. J. Hearn, The auroral distribution and its relation to magnetospheric processes, *Adv. Space Res., 13,* 17–27, 1993.

Elphinstone, R. D., K. Jankowska, J. S. Murphree, and L. L. Cogger, The configuration of the auroral distribution for interplanetary magnetic field B_z northward, 1, IMF B_x and B_y dependencies as observed by the Viking satellite, *J. Geophys. Res., 95,* 5791–5808, 1990.

Elphinstone, R. D., J. S. Murphree, D. J. Hearn, W. Heikkila, M. G. Henderson, L. L. Cogger, and I. Sandahl, The auroral distribution and its mapping according to substorm phase, *J. Atmos. Terr. Phys., 55,* 1741–1762, 1993a.

Elphinstone, R. D., D. J. Hearn, J. S. Murphree, L. L. Cogger, M. L. Johnson, and H. B. Vo, Some UV dayside auroral morphologies, in *Auroral Plasma Dynamics, Geophys. Monogr. Ser.,* vol. 80, edited by R. L. Lysak, pp. 31–45, AGU, Washington, D.C., 1993b.

Erlandson, R. E., D. G. Sibeck, R. E. Lopez, L. J. Zanetti, and T. A. Potemra, Observations of solar wind pressure initiated fast mode waves at geostationary orbit and in the polar cap, *J. Atmos. Terr. Phys., 53,* 231–239, 1991.

Feldstein, Y. I., and Y. I. Galperin, The auroral luminosity structure in the high-latitude upper atmosphere: Its dynamics and relationship to the large-scale structure of the Earth's magnetosphere, *Rev. Geophys., 23,* 217–275, 1985.

Feldstein, Y.I., and Y. I. Galperin, An alternative interpretation of auroral precipitation and luminosity observations from the DE, DMSP, AUREOL, and Viking satellites in terms of their mapping to the nightside magnetosphere, *J. Atmos. Terr. Phys., 55,* 105–121, 1993.

Feldstein, Y. I., V. G. Vorobjev, S. V. Leontyev, R. D. Elphinstone, I. I. Alexeev, and E. S. Belenkaya, Auroras in the polar cap, *IRF Sci. Rep. 209,* Swedish Institute of Physics, Kiruna, 1992.

Feldstein, Y. I., R. D. Elphinstone, D. J. Hearn, J. S. Murphree, and L. L. Cogger, Mapping of the statistical auroral distribution into the magnetosphere, *Can. J. Phys., 72,* 266-269, 1994a.

Feldstein, Y. I., A. E. Levitin, L. I. Gromova, L. A. Dremuhina, L. G. Blomberg, P.-A. Lindqvist, and G. T. Marklund, Electromagnetic weather at 100 km altitude on 3 August 1986, *Geophys. Res. Lett., 21,* 2095–2098, 1994b.

Frank, L. A., and J. D. Craven, Imaging results from Dynamics Explorer 1, *Rev. Geophys., 26,* 249–283, 1988.

Frank, L. A., et al., The theta aurora, *J. Geophys. Res., 91,* 3177–3224, 1986.

Galperin, Y. I., and Y. I. Feldstein, Auroral luminosity and its relationship to magnetospheric plasma domains, in *Auroral Physics,* edited by C.-I. Meng, M. Rycroft, and L. A. Frank, pp. 207–222,Cambridge University Press, New York, 1991.

Greenwald, R. A., K. B. Baker, J. M. Ruohoniemi, J. R. Dudeney, M. Pinnock, N. Mattin, J. M. Leonard, and R. P. Lepping, Simultaneous conjugate observations of dynamic variations in high-latitude dayside convection due to changes in IMF B_y, *J. Geophys. Res., 95,* 8057–8072, 1990.

Gusev, M. G., and O. A. Troshichev, Simultaneous ground-based observations of polar cap arcs and spacecraft measurements of particle precipitation, *J. Atmos. Terr. Phys., 54,* 1573–1591, 1992.

Hardy, D. A., L. K. Schmitt, M. S. Gussenhoven, F. J. Marshall, H. C. Yeh, T. L. Shumaker, A. Hube, and J. Pantazis, Precipitating electron and ion detectors (SSJ/4) for the block 5D/flights 6-10 DMSP satellites: Calibration and data presentation, *Rep. AFGL-TR-84-0317,* Air Force Geophys. Lab., Bedford, Mass., 1984.

Hones, E. W., J. D. Craven, L. A. Frank, D. S. Evans, and P. T. Newell, The horse-collar aurora: A frequent pattern of the aurora in quiet times, *Geophys. Res. Lett., 16,* 37–40, 1989.

Huang, C. Y., J. D. Craven, and L. A. Frank, Simultaneous observations of a theta aurora and associated magnetotail plasmas, *J. Geophys. Res., 94,* 10,137–10,143, 1989.

Iijima, T., and T. A. Potemra, The amplitude distribution of field-aligned currents at northern high latitudes observed by TRIAD, *J. Geophys. Res., 81,* 2165–2174, 1976.

Lyons, L. R., J. F. Fennell, and A. Vampola, A general association between discrete auroras and ion precipitation from the tail, *J. Geophys. Res., 93,* 12,932–12,940, 1988.

Lundin, R., L. Eliasson, and J. S. Murphree, The quiet-time aurora and the magnetospheric configuration, in *Auroral Physics,* edited by C.-I. Meng, M. J. Rycroft, and L. A. Frank, pp. 177–194, Cambridge University Press, New York, 1991.

Makita, K., C.-I. Meng, and S.-I. Akasofu, Transpolar auroras, their particle precipitations, and the IMF B_y component, *J. Geophys. Res., 96,* 14,085–14,095, 1991.

Meng, C.-I., Polar cap arcs and the plasma sheet, *Geophys. Res., Lett., 8,* 273–276, 1981.

Mizera, P. F., D. J. Gorney, and D. S. Evans, On the conjugacy of the aurora: High and low latitudes, *Geophys. Res. Lett., 14,* 190-193, 1987.

Murphree, J. S., and L. L. Cogger, Observed connections between apparent polar cap features and the instantaneous diffuse auroral distribution, *Planet. Space Sci., 11,* 1143–1149, 1981.

Murphree, J. S., S. Ismail, L. L. Cogger, D. D. Wallis, G. G. Shepherd, R. Link, and D. M. Klumpar, Characteristics of optical emissions and particle precipitation in the polar cap arcs, *Planet. Space Sci., 31,* 161–172, 1983.

Newell, P. T., W. J. Burke, C.-I. Meng, E. R. Sanchez, and M. E. Greenspan, Identification and observations of the plasma mantle at low altitudes, *J. Geophys. Res., 96,* 35–45, 1991.

Obara, T., M. Kitayama, T. Mukai, N. Kaya, J. S. Murphree, and L. L. Cogger, Simultaneous observations of sun-aligned polar cap arcs in both hemispheres by Exos C and Viking, *Geophys. Res. Lett., 15,* 713–716, 1988.

Parks, G. K., et al., Low-energy particle layer outside the plasma sheet boundary, *J. Geophys. Res., 97,* 2943–2954, 1992.

Peterson, W. K., and E. E. Shelley, Origin of the plasma in a cross polar cap auroral feature (theta aurora), *J. Geophys. Res., 89,* 6729–6736, 1984.

Potemra, T. A., Large-scale characteristics of field-aligned currents determined from the TRIAD magnetometer experiment, in *Dynamical and Chemical Coupling Between the Neutral and Ionized Atmosphere,* edited by B. Grandel and J. A. Holtet, pp. 337–352, D. Reidel, Norwell, Mass., 1977.

Sandahl, I., R. Lundin, and L. Eliasson, The hot plasma spectrometers on Viking, *KGI Tech. Rep., 035,* Kiruna Geophysical Institute, Kiruna, Sweden, 1985.

Sergeev, V. A., E. M. Sazhina, N. A. Tsyganenko, J. A. Lundblad, and F. Soraas, Pitch-angle scattering of energetic protons in the magnetotail current sheet as the dominant source of their isotropic precipitation into the nightside ionosphere, *Planet. Space Sci., 31,* 1147–1155, 1983.

Stasiewicz, K., Topology and position as a function of interplanetary magnetic field and magnetic activity: Comparison of a model with Viking and other observations, *J. Geophys. Res., 96,* 15,789–15,800, 1991.

Troshichev, O. A., and A. Nishida, Pattern of electron and ion precipitation in northern and southern polar regions for northward interplanetary magnetic field orientations, *J. Geophys. Res., 97,* 8337–8354, 1992.

Weiss, L. A., P. H. Reiff, R. V. Hilmer, J. D. Winningham, and G. Lu, Mapping the auroral oval into the magnetotail using Dynamics Explorer plasma data, *J. Geomagn. Geoelectr., 44,* 1121–1144, 1992.

Weiss, L. A., E. J. Weber, P. H. Reiff, J. R. Sharber, J. D. Winninham, F. Primdahl, I. S. Mikkelsen, C. Seifring, and E. M. Wescott, Convection and electrodynamic signatures in the vicinity of a sun-aligned arc: Results from the polar acceleration regions and convection study (Polar ARCS), in *Auroral Plasma Dynamics, Geophys. Monogr. Ser.,* vol. 80, edited by R. L. Lysak, AGU, pp. 69–80, AGU, Washington, D.C., 1993.

Zelenyi, L. M., R. A. Kovrazkin, and J. M. Bosqued, Velocity dispersed ion beams in the nightside auroral zone: AUREOL 3 observations, *J. Geophys. Res., 95,* 12,119–12,139, 1990.

Y. I. Feldstein, IZMIRAN, Akademgorodok, Troitsk, Moscow Region, 142092 Russia.

S. V. Leontjev and V. G. Vorobjev, Polar Geophysical Institute, Apatity, Russia.

P. T. Newell, Applied Physics Laboratory, Johns Hopkins University, Johns Hopkins Road, Laurel, MD 20723-6099. (e-mail: newell@oval.jhuapl.edu)

I. Sandahl and J. Woch, Swedish Institute of Space Physics, P.O. Box 812, Kiruna S-98128, Sweden.

(Received July 8, 1994; revised January 27, 1995; accepted January 27, 1995.)